5. TEST RESULTS

5.1 Introduction

Each of the 11 test elements (panels) were tested in accordance with SEAOSC testing protocol, as described in Section 2.1.4.1 of this thesis. The loading was based on a FME (or YLS) of 1″, as described in Section 3.2. Prior to installing each panel in the test rig, the fastener spacing was measured, and the hold-down installation to the end-wall studs was checked. After the test panel was installed, the LVDTs were zeroed and the DTs calibrated. Each DT was displaced to 1″, 2″, and 3″ and the operator verified the reading. A preload on the system required fitting the panel in between the stops on the guide beams and recorded. The test data were normalized during the data processing. Once the panel was installed between the guide beams, the anchor bolts and hold-down anchors were tightened, and the end-wall straps were nailed into position.

The testing sequence started with the displacement data acquisition system recording the LVT and DT data. Next, the actuator program was run to determine that the displacement data acquisition would envelope the entire test. Once the data were recorded, they were imported into an Excel spreadsheet from which the hysteresis loops were plotted. Using the hysteresis loops and tabulated data, the YLS, SLS and bilinear segments were determined for each test and each set of tests. The YLS point was the most difficult to determine. This point is defined as “the point in the force displacement relationship where the difference in the forces from the first and fourth cycles does not

exceed 5%" (SEAOSC, p. 2). The SEAOSC protocol is based on an assumption of the FME or YLS displacement, and the test is a series of stepped displacements determined as a multiple of the FME. The increment of the steps in the test is 25%. The cycles below the FME occur in sets of three; therefore, if the yield point is overestimated, as was the case in this test, then the yield point will occur during the first nine cycles where a group of four cycles of the same displacement do not exist. See the SEAOSC protocol in Appendix A and the displacement plots in Appendix D.

Based on the testing protocol, it is probably best to underestimate the FME point; however, the assumption needs to be within 25% of the actual FME point to accurately determine the YLS from the results. If the assumed FME is accurately estimated, it would occur after 17 cycles of the testing sequence, and it would occur in groups of 4 cycles at the same displacements to conform to the SEAOSC specifications.

The YLS points determined from this testing were verified by analyzing where the backbone curve slope changed by more than 5%. This point was verified with the tabulated data in the spreadsheets. Typically, I could not find 4 cycles as specified by SEAOSC, but I believe my results are within 10% of an accurate solution.

The SLS and bilinear segments discussed in Section 4.3 are more easily determined. The SLS point is the largest force and the displacement at that force. The bilinear segments were drawn from 0,0 to the positive and negative YLS and then from the YSL to the SLS. Once the YLS, SLS, and bilinear segments were drawn on the hysteresis loops, the displacement point of the YLS and SLS for both quadrants were plotted on the graph of the panel displacement versus time. It was easy to find the exact displacement point of the YLS and SLS on these plots, since there were only 3 to 6 cycles

in the vicinity of the displacement points. By plotting the displacement points versus time, the cycle number where the YSL and SLS occurred were determined and symmetry between the quadrants was verified. Appendix D contains plots from panels 2, 3, 4, 5, 6, 7, 9, 10 and 11.

5.2 Individual Panel Test Results

Set 1 consisted of panels 1, 2, 3, and 5. This set was constructed without any hold-down or plate modifications, as discussed in Section 4.2. For panel 1, no data are available for this panel because when the test was started, the data acquisition was not initiated to record the force and displacements. It was a good run-through for the system though in order to see how the wall was going to fail and how the setup had performed.

The physical connections of the two steel beams with stops on both ends held together well. Negligible play or movement was noticed in the connection. At the start of test of panel 1, the wall immediately rocked back onto the hold-downs as the end studs lifted up from the sill plate. This deflection was the result of the eccentricity between the hold-down anchor bolt and the sheathing fasteners along the end-wall. The end-wall studs rotated about their inside edge. As the displacements increased, the staples started to pull away from the framing and tear through the sheathing along the bottom edge of the panel. Viewing from the inside of the panel, I could see the sheathing begin to rotate around the center of the wall. As the cycles increased, the deflection of the top of the wall increased, and the separation of the end-wall studs from the sill plate increased and spread into the interior studs. No data were taken from this test. The failure mechanism observed was similar to those found by Shipp et al. (2001), who had also witnessed the shear walls first failing along the bottom edge of the sheathing. Figure 5.1 shows a photo

Figure 5.1. Panel 1 fastener and sheathing failure at the sill plate.

of this failure. After testing panel 1, it was decided to test three 4′ wide x 8′ tall panels constructed to panel 1 specifications and then try to improve the performance of the wall by controlling the uplift of the end-wall studs.

When this panel 2 was set up, the connection to the anchor bolts at the bottom and the frame holding the top of the panel in place were tight. This tightness was probably due to the panel not being square and then forced into the testing rig. The panel demonstrated a higher initial stiffness than other panels. Since this panel was constructed (1999) and was stored in the enclosed testing laboratory at the University of Utah until the test date, the moisture content was probably half of some of the newer panels. In addition it was 1/8″ out of square, which caused it to be forced or preloaded into the test rig; the preload was 120 pounds. These two factors both contributed to the 22% to 45% greater elastic stiffness in the panel compared to panels 3 and 5.

The following properties were determined from the hysteresis loop in Appendix D. This panel recorded a YLS capacity of 3.1 kips at a displacement of 0.58″. The yield load occurred at almost one-half of the assumed yield displacement load after seven test cycles (Appendix D). The yield load would have occurred after 32 cycles if the yield point had been estimated accurately, since the program's initial displacement would be lower. Although the yield point could not be determined to the exact letter of the SEAOSC definition, it can be seen from the hysteresis loop that degradation in stiffness occurs after this point and is verified from the tabulated data of the force deformation.

The SLS capacity of Panel 2 was 3.7 kips at a displacement of 1.9″. After reaching the ultimate load, the panel's strength degraded rapidly. The staples in the

bottom of the panel tore through the sheathing along the bottom edge back to the first interior stud. This failure proceeded rapidly toward the center stud but not up the length of the end-wall studs. Failure of the staples up the vertical studs was prevented due to the double row of staples along the two end-wall studs at each end. The two rows of staples provided additional strength and prevented rapid failure up the end-wall studs. Appendix D shows how the positive displacement of the SLS point was reached 24 cycles earlier in the test than the negative displacement. The positive SLS point came after only 17 cycles, and the negative displacement SLS point occurred after 40 cycles or over halfway through the testing protocol. This difference must have occurred due to a premature failure of the wall's ability to carry the tension loads on the west side of the panel; positive displacements were to the east. Only panel 3 showed a similar pattern; other tests did not show this discrepancy.

Panel 2 failure elements were: (1) the failure of the single row of staples along the bottom of the panel and (2) the sill plate splitting. The sill plate split from the cross-grain bending along the length sill, from the outside edge where the sheathing was fastened back to the interior anchor bolts (Figure 5.2). The sill plate was split from its end back to the center stud.

The staple failures along the bottom edge of the panel came from the staples cutting through the OSB. The staples worked themselves out of the framing 1/4″ and did not shear off in the framing. The failure mode was the sheathing crushing and disintegrating around the staple leg. From this behavior, it was determined that this size staple would perform well in thicker sheathing. Fastener fatigue was a common failure in all of the researched reviewed in Section 2 and the reason for one of the papers (He et al.

Figure 5.2. Panel 2 sill plate splitting along centerline.

1999) to design a less demanding cyclical test protocol. The 16 gauge 2″ staples used for this testing did not fatigue when coupled with the 7/16″ sheathing tested.

Panel 3 was easily installed with a preload of only 47 pounds since it was square to 1/16″. This panel was built in 1999 and stored under the same conditions as panel 2; therefore it had similar moisture content. The test results were comparable to the test results of panel 2 and had the same fastener failure mechanisms as panel 2. Like panel 2, this panel failed at the staple connection to the sill plate as well as the end-wall studs that fractured; however, the sill plate did not split on this panel. The YLS capacity was 3.0 kips at 0.70″ displacement. The same difficulties in determining the YLS point of panel 2 occurred with panel 3. However it is obvious from the reduced strength and break in the bilinear segments that the values selected were accurate. The YLS point occurred at cycle 10.

For panel, 3 SLS capacity was 4.8 kips at a displacement of 1.8″. The SLS points in the positive and negative quadrants of the hysteresis loop occurred 11 cycles apart, which is closer together than panel 2, but farther apart than other tests. The failure of the panel began in the lower corners of the panel and spread inward towards the center of the panel. It is unclear at what cycles the end-wall studs fractured, as shown in Figure 5.3. The fasteners did pull out of the framing along the end-wall studs, and the sheathing's connection to the sill failed from the fasteners shredding the sheathing in the lower corners. Since the sill plate stayed intact, the sheathing failure spread upward along the end-wall studs despite having two rows of fasteners. The hysteresis loop for this panel, which is representative of the first test group, is shown in Figure 5.4.

Figure 5.3. Panel 3 sheathing tearing and end wall stud crack.

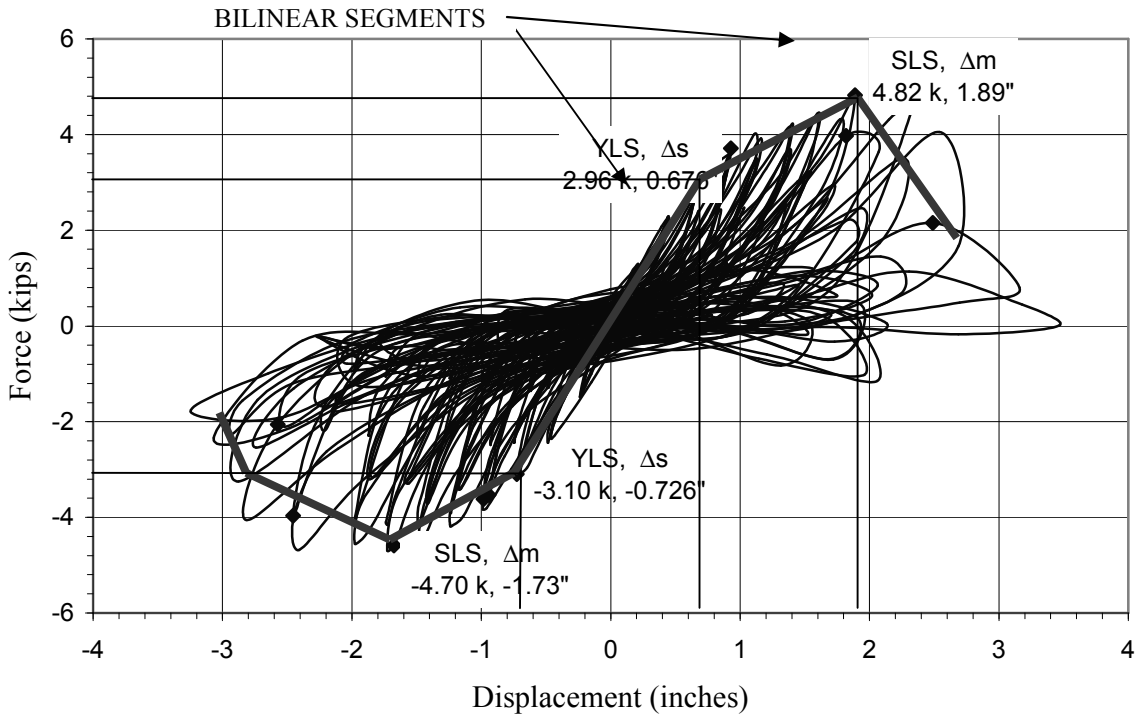

Figure 5.4. Hysteresis load-displacement curves panel 3.

Panel 5 was constructed only one day prior to the test. The studs were wet had a higher moisture content than the other panels. The panel was installed with low to zero preload since it was square. The panel was less stiff than the previous two panels of this type. This reduced stiffness was assumed to be from the higher moisture content in the studs used for this panel. The YLS capacity was 2.4 kips at a displacement of 0.67″, respectively, with the strength roughly 20% lower than panels 2 and 3 that corresponds to the C_m (reduction for moisture) factor of 0.8 in the NDS design code. The SLS capacity was 4.1 kips at a displacement of 1.7″. The displacement was from 10% to 20% lower than panel 3, yet 10% greater than panel 2. The YLS and SLS points occurred within two

cycles of one another. The failure was restricted to the bottom row of staples along the sill plate, the end-wall studs, and the first interior studs lifted off the sill plate.

Panel 4 was constructed identically to panels 1, 2, 3, and 5, with the exception that a strap was added to connect the a-bolt beneath the sill along the underside of the sill plates and up the side of the panel. The purpose of this strap was to reduce uplift between the end-wall studs and the sill plate, thus reducing the stress on the staples in the bottom corners of the panels. From this test the panel produced the YLS capacity of 3.3 kips at a displacement of 0.96″ after three cycles at the yield displacement. The SLS capacity was 5.3 kips at a displacement of 2.4″. The SLS points occurred within four cycles of each other, demonstrating improved symmetry in the panel's strength to the YLS. These results represent a 10% increase in strength, although the stiffness of the element was not improved. The improved YLS load and displacement occurred from only the addition of the end-wall strap to the panel. The results are shown in Figure 5.5.

The strap caused the sill plate to flex along its length at the sill plate's ends during uplift, relieving stress on the staples. During compression on the panel's end-wall studs, crushing of the sill plate occurs and the stress on the bottom corner staples is increased. Figure 5.6 shows photos of the panels displaced at the end of the test cycle. Figure 5.6 also demonstrates the effects of the strap; note the sill plate curling upward. The failure mechanism for the test was the sill plate cracking, not splitting along its length, due to cross-grain tension and the sheathing pulling away from the studs as the staples worked out of the framing. This type of failure will absorb more energy, which can be seen on the hysteresis loop for this test in Figure 5.5. The backbone curve from the loop has a

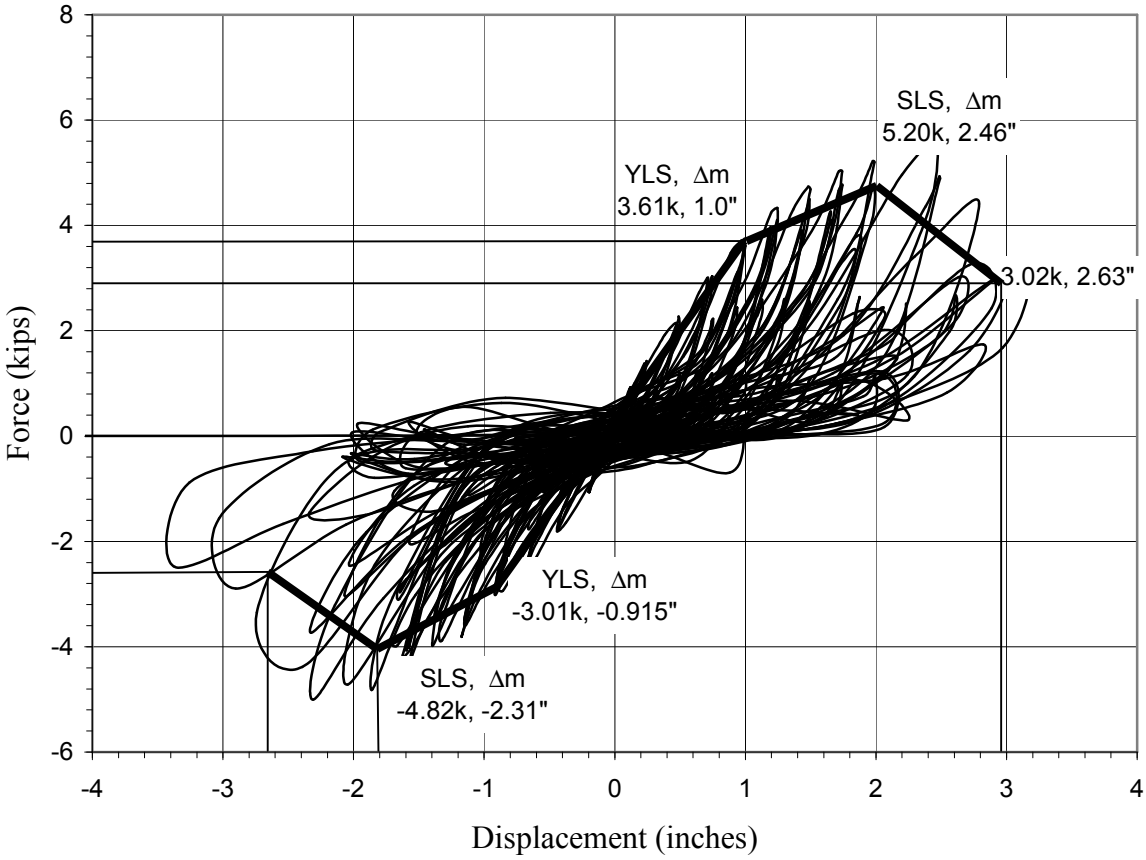

Figure 5.5. Hysteresis load displacement curve panel 4.

positive slope after yield and a more shallow decay after the ultimate load has been reached.

Panel 6 had the same configuration as panel 4. In addition the bottom sill was reinforced with blocking between the studs (see Appendix B). The blocking served two purposes: (1) the interior studs would separate from the sill plate in the latter stages of the previous tests and would now have blocking clamping them in place on each side; and (2) the bottom row of staples along the base of the wall could now have two rows of staples at 2 ½″ on center. Panel 6 had an opening in the one outside end-wall stud, and during

Figure 5.6. Failure components panel 4.

tension, the blocking piece installed in the 18″ space would separate from the stud below causing the wall to have a reduced stiffness. Even with this deficiency, the test results showed an increase in stiffness and YLS capacity. The YLS capacity was 3.4 kips at a deflection of 0.88″. The SLS capacity was 5.2 kips at a deflection of 2.3″. Both the YLS and SLS in both quadrants occurred on the same cycle: (1) the YSL after 17 cycles and (2) the SLS after 39 cycles. This symmetry suggests that no premature failures occurred on one side of the panel and not the other. The SLS capacity had no increase over panel 4, even though the sill plate was blocked. This lack of SLS increase was due to the single row of staples along the top plate. By blocking the sill plate, the failure mechanism simply shifted to the top plate at a load within 10% of panel 4. It was clear from this test that two rows of staples around the entire panel would be required to maximize the panel's performance.

Panel 7 represented the first panel constructed with all three modifications (Figure 5.7). The panel was constructed with two 2″ x 4″ studs at the wall ends, top and bottom plates, which were face-nailed together with 10d common nails at 6″ on center. The interior studs, spaced at 16″ on center from the end studs, were single 2″ x 4″ members. The sheathing was 7/16″ thick OSB stapled at 2 ½″ on center to each 2″ x 4″. The double top and bottom plates, and end-wall studs provided two rows of staples around the entire perimeter of the panel. At the base of the panel, PHD2 hold-downs were installed at each end and a ST6236 strap was installed around the anchor bolt and up the side of each end studs. The base of the wall was secured with five 5/8″ diameter all-thread bolts anchored into the concrete foundation. The all-thread anchor bolts passed through both studs and using a 2″ square washer clamped down on the double sill plate holding it in

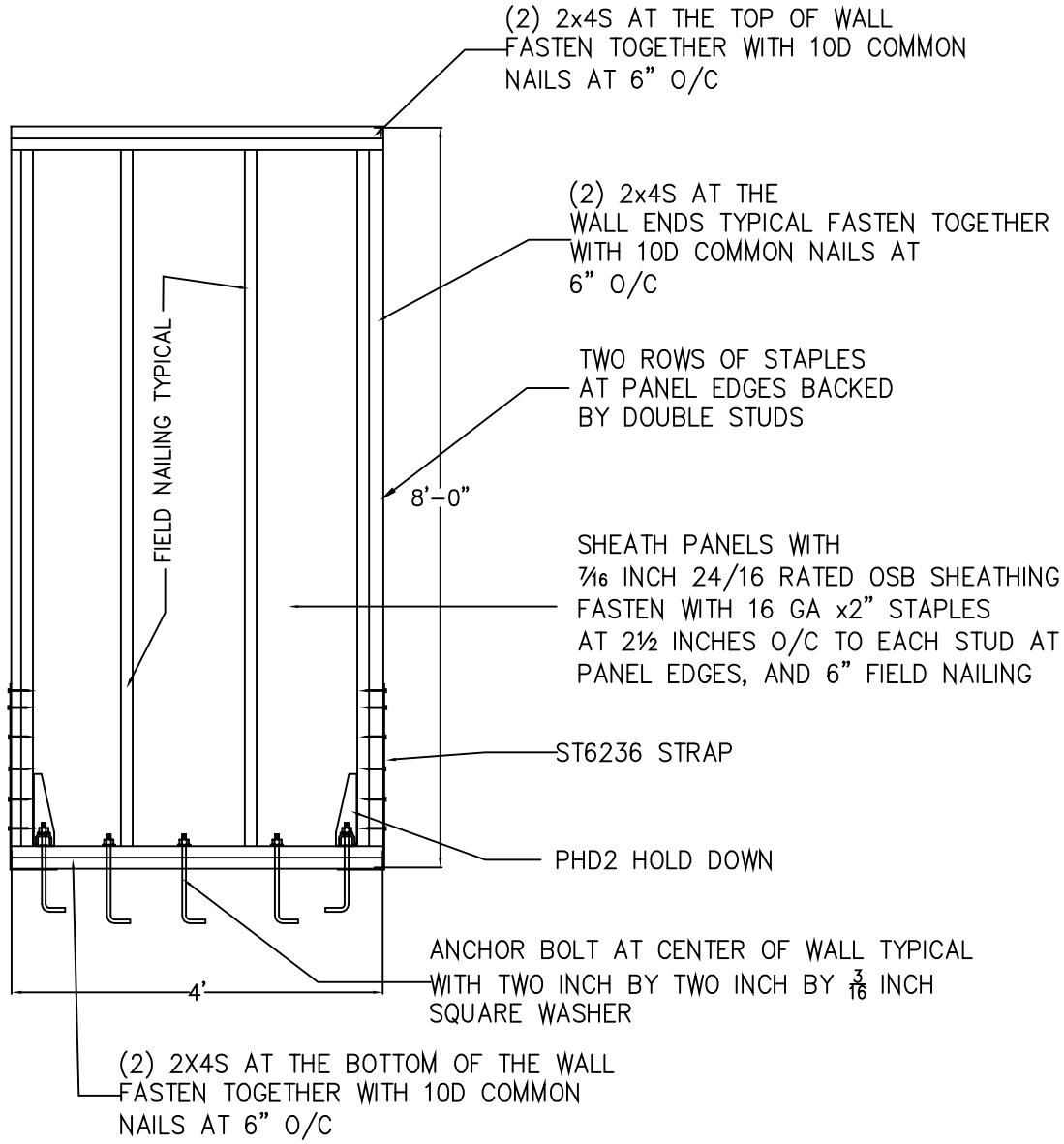

Figure 5.7. Panels 7, 8, and 9 elevation drawing.

place against the concrete. Figure 5.8 shows the base configuration and Figure 5.9 shows a close up of the strap to threaded rod connection. Panel 7, with the new configuration, had better performance than the previous tests. The YLS capacity was 3.9 kips at a displacement of 0.95″ after 17 cycles. The SLS capacity was 6 kips at a displacement of 2.4″ occurring between cycles 52 and 56. These capacities represent a 30% increase in yield strength and a 60% increase in ultimate strength over the best performance of the standard construction panels used in tests 2, 3, and 5. The increase in ultimate strength and the broader back-bone curve demonstrated the modifications to the base of the shear

Figure 5.8. Base configuration of panel 7.

wall that prevented premature failure of the wall components. Failures occurred with the end studs splitting, the sill plate splitting, and the sill plate crushing where the ST strap held the end-wall studs down, with several components of the hold-down failing at a calculated uplift of 12 kips (see Figures 5.9, 5.10, and 5.11). The hold-down component failures included the screws bending and shearing off at the heads, the sill plate crushing under the toe of the hold-down, and the hold-down structure beginning to come apart. During the entire test, the sheathing fasteners showed little sign of failure. Some staples began to work their way out of the studs, but the wall sheathing remained fixed to the base of the shear wall. The failure mechanism of the panels shifted from failing at the sheathing where there were only single rows of fasteners to failing at the sill plate, end-wall studs, and hold-down components. By improving the fixture of the base of the shear wall, the panel strength and ductility of the element was improved. Figure 5.12 shows the hysteresis loop for this panel.

The benefits of the added strap to the hold-down configuration of panel 7 were obvious with the increase in YLS and SLS capacities. This panel demonstrated that having two 2″ x 4″ for a sill plate and two rows of nailing around the entire panel would improve the panel's performance. The eccentricity from the hold-downs causes higher stress on the. fasteners in the panel's lower corners and cross-grain bending in the sill plate. The metal strap and double sill fastened together with the anchor-bolts and 2″ square washers compenstated for these stresses. The failures for panel 7 occurred in the end-wall studs, double-sill plate, and hold-downs; the panel sheathing was optimized. Improvements can still be made in the panel designed for this test. The first would be to champher the end of the bottom sill plate so the strap is bent at two locations with two

Figure 5.9. End-wall stud strap panel 7.

Figure 5.10. End-wall stud, hold-down, and sill failure panel 7.

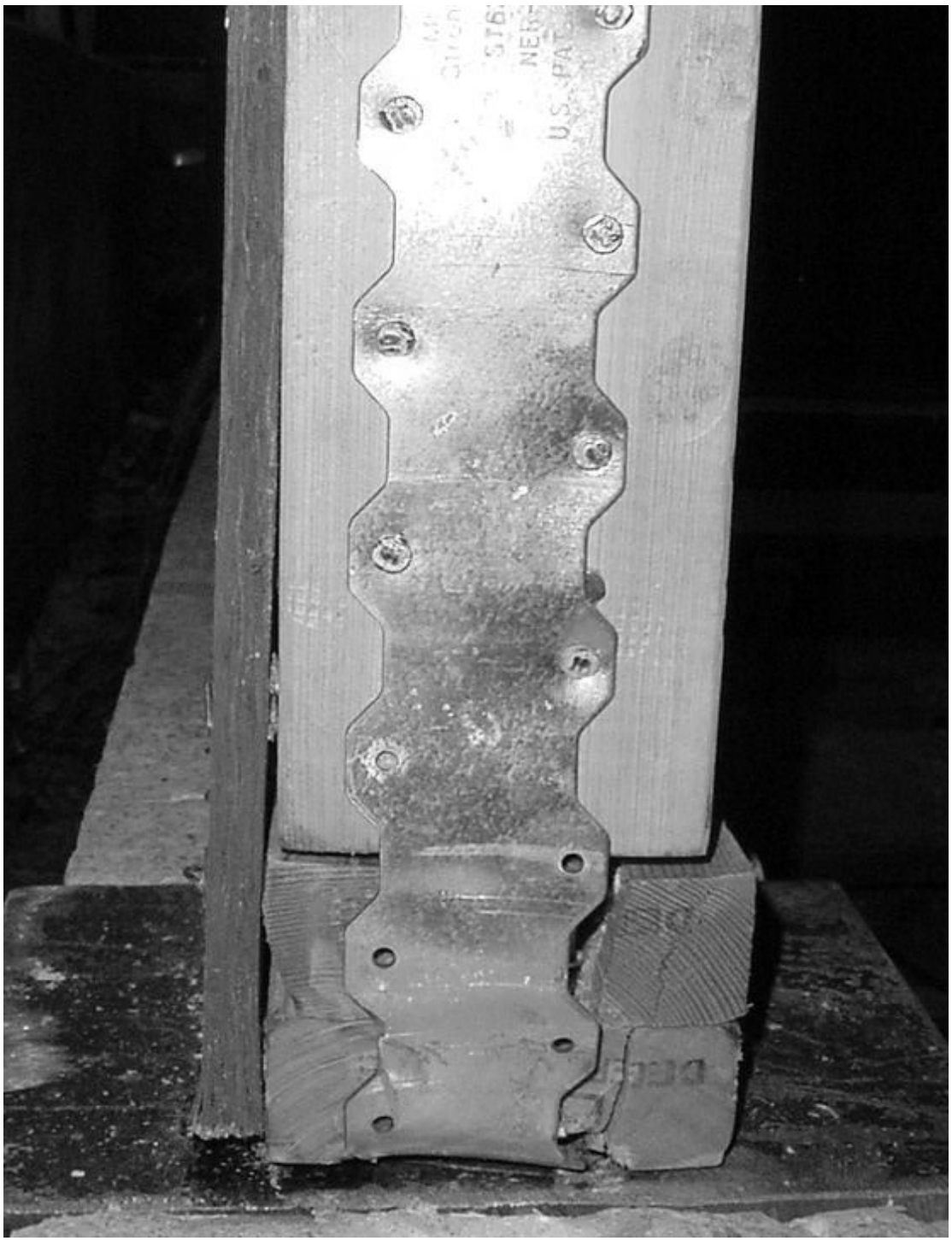

Figure 5.11. End-wall strap crushing the sill plates, panel 7.

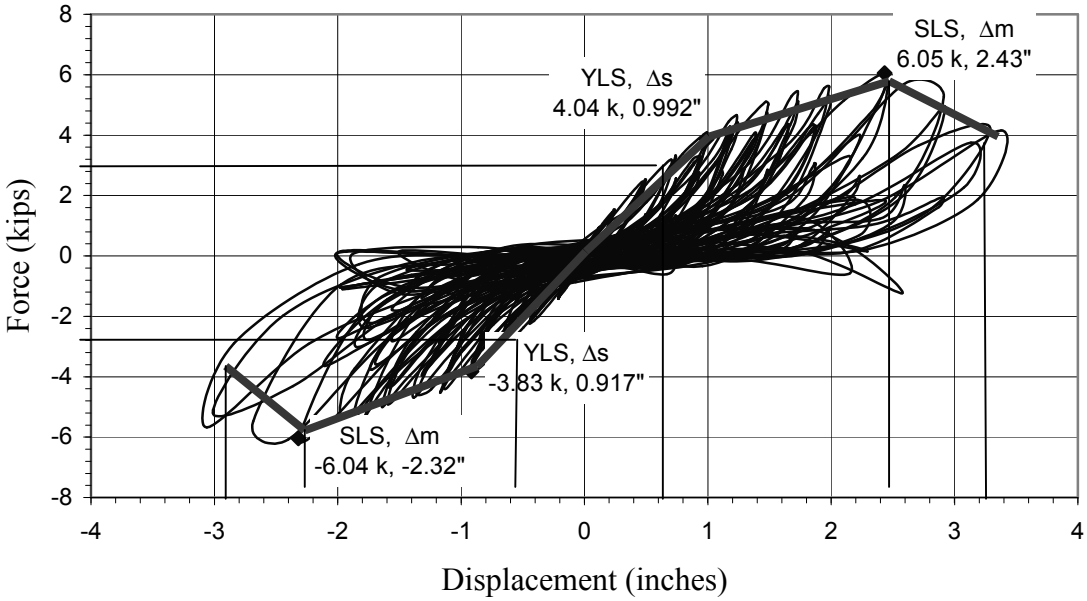

Figure 5.12. Hysteresis load displacement curve panel 7.

45° bends in lieu of one 90° bend. This champher will also improve the contact bearing strength of the sill plate, since the strap would not be bearing on the corner and would be perpendicular to the sill plate grain. Instead, the strap would bear at a 45° angle to grain. Another improvement would be to use a wider strap to utilize the full width of the sill plate. Limiting the uplift of the end-wall studs would marketedly reduce top of wall deflection, especially on walls with h/w ratios of 2 or higher.

Panel 8 was constructed identically to panel 7. This test was run erroneously with the hydraulics on low pressure, therefore, the panel was not tested properly. The hysteresis curve did portray a response similar to test 7. The data for this panel are not presented.

Panel 9 was constructed identically to panels 7 and 8. The test results from this panel were close to the result of panel 7. The YLS capacity was 3.9 kips, at a displacement of 1″ and the SLS capacity was 5.9 kips at a displacement of 2.4″. With both the YLS and SLS within 10% of one another there was no need for a third test per SEAOSC specifications. The YLS and SLS occurred at cycles 16, 17 and cycles 52 through 56, respectively, and both points occurred at the same cycle number as panel 7 (see Appendix D, D.12, and D.14).

Panel 9 also failed with the same failure mechanisms as panel 7. The hold-down device failed and the wood sill plates and end studs split and cracked. The studs pulled away from the sill due to the hold down failure. The hold-down twisted and the screws sheared and bent. The staples held the sheathing connected to the wood framing. The performance of this panel confirmed the results in Panel 7.

Panel 10 was an 8′ x 8′ panel constructed from two 4′ panels bolted together with five ½″ diameter all-thread bolts. The bolts were evenly space along the four 2″ x 4″ end studs, (see Appendix D). The combined 8′ panel had hold-downs at each end 8′ apart. The top plates were blocked so there were two rows of staples along the top edge of the two 4′ x 8′ sheets of OSB (the OSB was applied vertically). The sill plate was blocked and two rows of staples were applied along the base of each panel. The result of the test was a YLS capacity of 9.8 kips at a displacement of 1.44″. The SLS capacity was 11.9 kips at a displacement of 2.4″. The SLS displacement was almost identical to test results of panels 4, 6, 7, and 9. Also the SLS capacity was twice that of panels 7 and 9, differing from the results of Shipp et al. (2001) who found only a 33% increase in the 8′ panels from the 4′ panels (the panels tested did not have modifications to account for the stresses

induced by the eccentric hold-downs). The YLS and SLS occurred at cycles 32 through 34 and 52 through 56, respectively. The SLS point occurred at the exact same cycles as panels 7 and 9. Panel 10 demonstrated that the modifications and components changed the behavior of the shear wall from a response similar to a cantilever beam element to a response similar to a shear wall element.

As panel 10 was cycled through the test protocol, the single panel began to react to the loading as two separate panels. Despite the ½″ diameter all-thread, the discontinuity in the plates caused the interior studs to independently shift. This bent the bolts and the corners of the sheathing in the center of the panel began to pull away from the studs as the staples pulled out. Next the interior studs in the center of the panel began to pull up off the sill plate. The hold-downs also failed as the screws deformed and sheared, and the bracket itself came apart. It appears the load on the hold-downs was greater than the load in the 4′ panels, even though the higher load should have been canceled out by the lower aspect ratio. At loads beyond the YLS point is when the 8′ panel began to act as two independent 4′ panels increasing the load on the hold-downs. The break-up of the two panels possibly occurred because the top and bottom plates were discontinuous and the sheathing splice at the center of the wall was vertical. This failure mechanism also occurred in the tests performed by Ming and others, so it is uncertain if continuous top plates alone would prevent this failure.

Panel 11 was constructed and tested identically to panel 10. The panel performed similarly to panel 10 with a YLS capacity of 9.1 kips at a displacement of 1.5″. The SLS capacity was 12.3 kips at a displacement of 2.8″. Only the positive quadrant revealed load deformation data after the YLS due to a premature failure on the east side of the

panel. Therefore only the positive quadrant values are presented. The values verified the capacities determined from panel 10.

In summary the 8′ panels pushed the limit of the hold-down configuration that was developed. The failure mechanism of the panels began with the panels acting as two independent components. Additional strength and ductility could be developed out of this configuration with the sheathing installed with the long direction perpendicular to the framing members and the edges solid blocked. This sheathing installation and a continuous top and bottom plate should be standard construction practice on long shear walls. The hold-down system developed for the 4′ panels would perform well on longer walls, where additional attention to the adjoining panel joints would aid in increased performance.

Displacement data acquisition for the tests was described in Section 3.3. The data acquisition recorded the following displacements: (1) panel uplift, measured on each end of the panel; (2) hold down uplift, was measured on the east end of the panels; (3) top of the wall displacement measured by both the actuator and the DT 5; (4) base lateral movement, measured with two LVDTs numbers 10 and 13.

The panel's top lateral displacement was measured by the actuator and DT 5 for panel 2 are compared in Figure 5.13. As shown by the graph the displacements measured parallel each other. There about six instances in the later cycles where the displacement measured by the actuator arm exceeds that of the DT. This can be attributed to the higher deflections at the 2 Hz frequency creating a lag in the DT data acquisition.

The end-wall uplift was measured with DT8 and DT9. These measurements

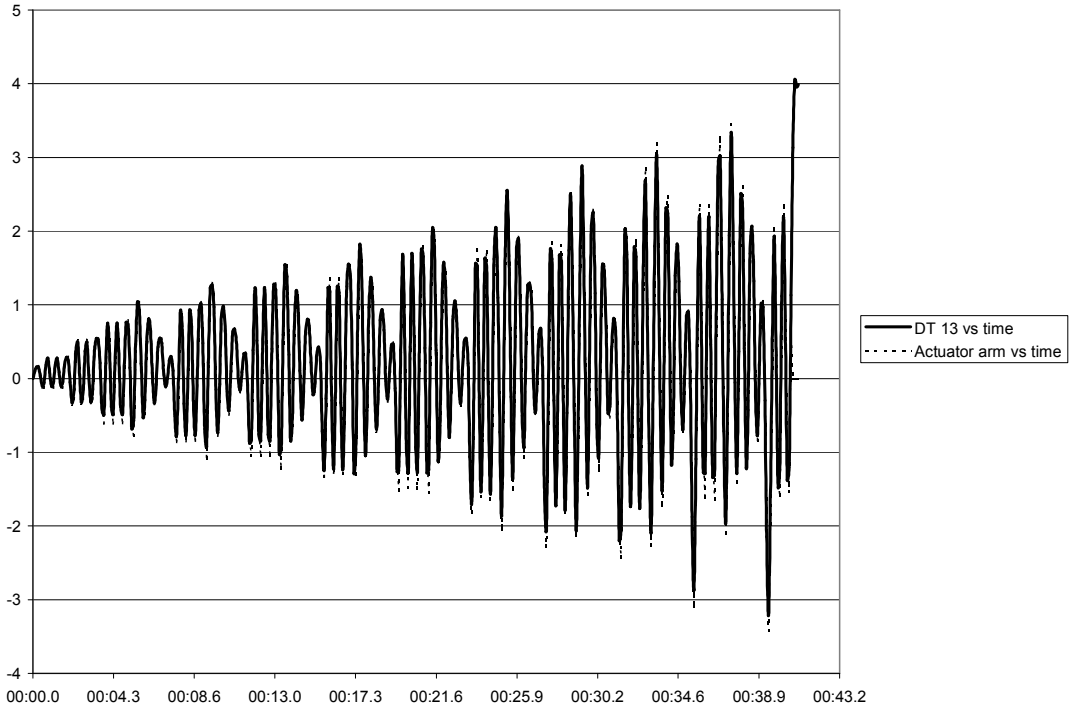

Figure 5.13. DT13 and actuator arm displacement versus time.

mirrored one another, that is, the maximum downward displacements matched, the opposite maximum uplifts matched, and both occurred simultaneously. This symmetry demonstrated that the instruments were set up and working properly. DT9 on the west side was consistently higher by approximately ¼″ than DT8. This was because the load was applied from the west end of the panels. This was the same side as DT9 and the testing began with the actuator pushing from west to east in its initial stroke. Regardless, DT8 and DT9 provided valuable information on the improved performance of the hold down configuration. Figure 5.14 shows that as ultimate loads were increased, the hold-down modifications decreased the end-wall uplift. Correlating this back to Figure 4.4 shows how by reducing the hold-down deflection we have significantly limited the overall drift of the panel. Figure 4.4 also shows how the hold-down deflection term increases in significance as the aspect ratio increases.

To verify there was no lateral sliding of the shear panel, LVDTs 10 and 13 were attached to the sill plate. The maximum measurements recorded by these instruments were in the hundreths of inches, which demostrated the panel was properly restrained laterally.

Although the displacement recorded demonstrates the improved panel performance, a method to quantify the improved performance of the new hold-down configuration within code parameters is desirable. The AC130 performace criteria was applied to the data to determine the design loads of the panels. This provides a method of determining the design loads that can be compared to the allowable strength design loads used in the new building-design construction codes.

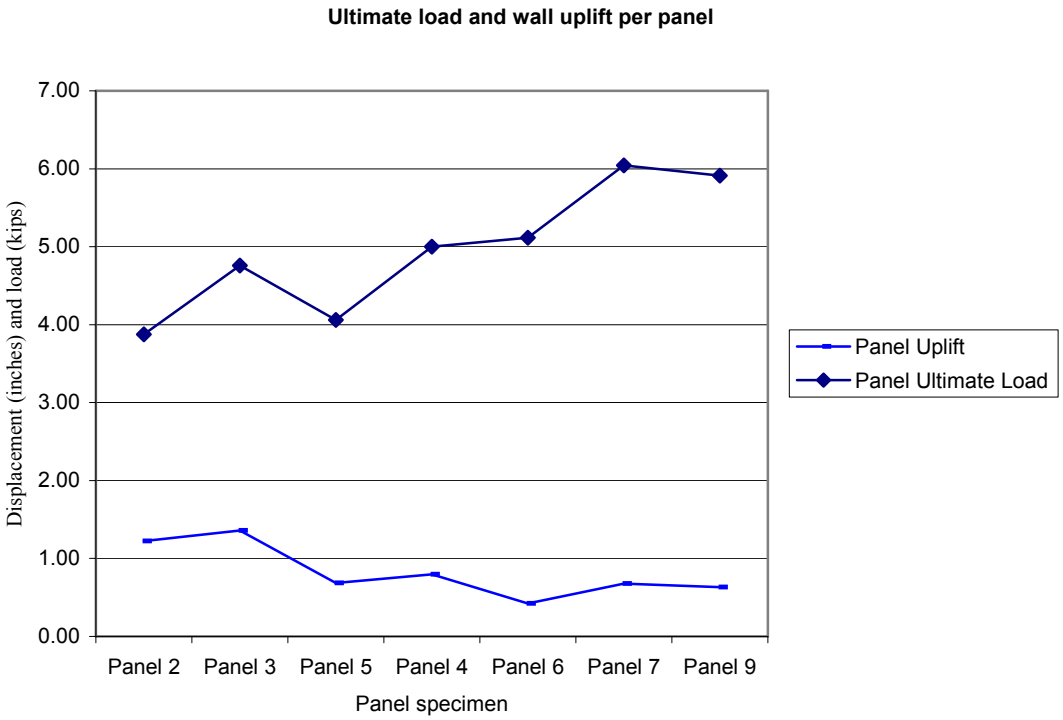

Figure 5.14. Ultimate load and wall uplift per panel.

5.3 AC130 Allowable Design Loads

The hysteresis loops from each test are provided in Appendix D. Table 5.1 shows the results that were analyzed according to AC130 specifications. The calculations are presented in Appendix E. The allowable stress design loads are calculated by taking the lesser of two conditions: (1) the load corresponding to Δ_s as described in Section 2.4 or (2) the ultimate capacity with a factor of safety of two. The controlling condition was the load corresponding to Δ_s/1.4 (Condition 1). The results of the AC130 analysis of the test results are shown in Table 5.1. Table 5.2 panels 2, 3, and 5 were the configurations found in standard construction practices. The results from the first three tests (Set 1), resulted in an average load of 336 plf (see Table 5.2 and the last column of Table 5.1). This is a 7% increase over the design loads found in NER 272 for 7/16″ panels with 16 gauge staples at 2 ½ icnhes on center. This demonstrates that the NER 272 loads, that are based on the old proportional limit equations and some static pushover tests are appropreate. The data from the first set (panels 2, 3, and 5) are scattered. Results in Table 5.1 show how the individual panel results vary for the first three panels tested in Set 1. For a single panel of the same construction the results vary by as much as 54 plf. This inconsistant data can be attributed to panel 2 being out of square, and of the higher moisture content of panels 3 and 5.

The results shown in Table 5.1 demonstrate that, as the panels were systematically modified, there was the progressive increase in the allowable strength design load. The allowable design loads increased 20% from panels 2, 3, and 5, to that of panels 7 and 9. The YLS capacity and SLS capacity increased progreessively from panels 2 through 6.

Table 5.1. Tabulated Test Results

Panel #	UBC Design Load (kips)	UBC Design displ (in)	Yield Load (YLS) (kips)	Yield disp (in)	K yield (kip / in)	Ultimate load (SLS) (kips)	Ultimate displ (in)	Allowable design load from tests per AC130 (kips)	design load from tests per AC130 (plf)	
Panel 2	1.25	0.20	3.1	0.58	5.26	3.9	1.55	1.57	393	
Panel 3	1.25	0.20	3.0	0.70	4.32	4.8	1.81	1.46	366	
Panel 5	1.25	0.20	2.4	0.67	3.58	4.1	1.65	1.36	339	
Panel 4	1.25	0.20	3.3	0.96	3.46	5.0	1.95	1.43	357	
Panel 6	1.25	0.20	3.4	0.95	3.61	5.1	1.78	1.50	375	
Panel 7	1.25	0.20	3.9	0.95	4.12	6.0	2.38	1.86	464	
Panel 9	1.25	0.20	3.9	1.0	3.85	5.9	2.38	1.82	455	
Panel 10	2.51	0.15	9.8	1.40	7.00	11.9	2.37	3.39	424	
Panel 11	2.51	0.15	9.4	1.425	6.60	12.34	2.81	2.86	357	
Panel #	displ @ AC130 design loads from Ky (Δdsg)	Δm= 1.4 x 0.7 x R x Δdsg	Δm (UBC design loads)= 1.4 x 0.7 x R x Δdsg	Yield Load (YLS) (kips)	Ultimate load (SLS) (kips)	Load Factor SLS / UBC design loads	Load Factor SLS / AC130 design load	Load Factor SLS / YLS	AC130 Design load from Set calculations	% Increase AC130 vs. UBC design loads
Panel 2	0.30	1.61	1.05	3.1	3.9	3.1	2.5	1.3	1.35	7%
Panel 3	0.34	1.83	1.05	3.0	4.8	3.8	3.3	1.6	1.35	7%
Panel 5	0.38	2.05	1.05	2.4	4.1	3.2	3.0	1.7	1.35	7%
Panel 4	0.41	2.23	1.05	3.3	5.0	4.0	3.5	1.5		14%
Panel 6	0.42	2.24	1.05	3.4	5.1	4.1	3.4	1.5		20%
Panel 7	0.45	2.43	1.05	3.9	6.0	4.8	3.3	1.5	1.76	40%
Panel 9	0.47	2.55	1.05	3.9	5.9	4.7	3.2	1.5	1.76	40%
Panel 10	0.48	2.61	0.83	9.8	11.9	4.8	3.5	1.2	3.27	30%
Panel 11	0.43	2.33	0.83	9.4	12.3	4.9	4.3	1.3	3.27	30%

This increase represents the additonal ductility and strength added to the system at higher displacements. The remaining 4′ panels 7 and 9 have the full hold-down modifications and have increased allowable design load of over 30% above panels 2, 3, and 5; and 40% greater than the UBC allowable design loads.

In Table 5.2 the far right hand column of the last two rows shows that panels 10 and 11 (8′ panels) have a lower increase of AC130 design loads than the 4′ panels. This is because of the construction of the panels. Each panel was originally two 4′ panels with single top and bottom plates. Next, the panels were modified by blocking the plates and bolting the end-wall studs together in the center of the panel. The test description explained the failure mechanism, and it was clear that after the panels reached their yield point they began to behave as two separate panels. This emphasizes the need to use a single 3x-boundary member for the center stud when sheathing is installed vertically, or use three 2x studs face nailed at a spacing that can withstand the ineleastic loads in plf of two 4′ sections.

The load factors for each individual panel is SLS capacity divided by the allowable stress design level capacity (F_{SLS} / F_{ASD}). The load factor is calculated from the average SLS for each and is shown in Table 5.1. The cyclical test produced load factors ranging from 3 to 4.8 greater than UBC design loads. The greatest increase occurred in the SLS values. The load factors produced from these tests demonstrated the performance gain. The load factors found in other cyclical loading test (Rose 1998) were in the range of 2 to 2.5. The load factors calculated in this testing signified a potential performance gain using 16 gauge x 2″ staples and OSB, with modified hold-down configurations.

Table 5.2. Calculations of Acceptance Criteria 130 Design Loads

Set #1 Ave of Panels # 2,# 3,&# 5			
	Force (kips)	Displ (in) Δ	
AC130 design	1.3	0.3	
YLS	2.8	0.7	From force deformation data, typica
SLS	4.2	1.67	From force deformation data, typica
$\Delta m = \Delta SLS =$		1.67	
$\Delta s =$	1.88	0.434	Calculated per AC130.
K(yls)=	4.344	k / inch	Calculated per AC130.
K (sls)=	1.378	k / inch	Calculated per AC130.
	design load	est displ	
ASD load per AC130=	1.35	0.3098	in From force deformation data.
in plf =	336		
ductility $\Delta SLS/\Delta YLS$ =	2.57		
ductility $\Delta SLS/\Delta ASD$ =	5.39		
Energy disapation =	4.52	kip x inches	
%Drift @ SLS =	1.74%	Within Code drift limit	
Drift limit per UBC 1630.10.2	2.50%		
Set #2 Ave of Panels # 7,& # 9			
	Force (kips)	Displ (in) Δ	
AC130 design	1.76	0.4	% inc over set 1
YLS	3.9	1.0	38.3
SLS	6.0	2.4	41.3
$\Delta m = \Delta SLS =$		2.4	
$\Delta s =$	2.46	0.618	
K(yls)=	3.98	k / inch	
K (sls)=	1.48	k / inch	
	design load	est displ	
ASD load per AC130=	1.756	0.4411	
in plf =	439		30.4
ductility $\Delta SLS/\Delta\Psi LS$ =	2.42	3.654	
ductility $\Delta SLS/\Delta ASD$ =	5.39		
Energy dissipation =	8.82	kip x inches	
%Drift @ SLS =	2.48%	Within Code drift limit	
Drift limit per UBC 1630.10.2	2.50%		
Set #3 Ave of Panels # 10,& # 11			
	Force (kips)	Displ (in) Δ	
AC130 design	3.27	0.5	
Yield	9.6	1.4	
Ultimate	12.1	2.6	
$\Delta m = \Delta SLS =$		2.6	
$\Delta s =$	4.58	0.673	
K(yls)=	6.80	k / inch	
K (sls)=	2.15	k / inch	
	design load	est displ	
ASD load per AC130=	3.268	0.4805	
in plf =	409		
ductility $\Delta SLS/\Delta YLS$ =	1.83		
ductility $\Delta SLS/\Delta ASD$ =	5.39		
Energy dissipation =	19.59	kip x inches	
%Drift @ SLS =	2.70%	Exceeds Code drift limit	
Drift limit per UBC 1630.10.2	2.50%		

The AC130 design criteria uses the lesser of the drift limit and ultimate load limit. The ultimate load limit has a factor safety of two, so the minimum load factor that would be calculated from the criteria is two. The test results calculated load factors around 4 with the modified panels. This is desirable when the wood shear wall structures are designed with an R value of 5. The greater the overstrength factor combined with the ductility the better reliability and energy dissipation of the system. The reason the load factors exceed two is that the computed design loads from test data were all controlled by drift.

The drift limitations required by UBC 1630.10.2 (1997) were met by all the test panels with the exception of the panels 10 and 11. The construction of these panels and the way they failed by acting as separate components past yield, was the primary cause of the higher drift. The drift limitation of 2.5% of the story height allows for almost 2½″ of drift per 8′ story. Test panels 7 and 9 reached this limit at their SLS capacity. Rose (1998) discusses whether or not this limit should be decreased to limit architectural damage in the elastic range, based on the veneer or other finishes. A benefit of performance-based design is that these design parameters would all be decided at project initiation and designed into the shear wall system, and not checked as an ad hoc design requirment. Using current design codes: if Δ_m was found to be unacceptable in terms of performance, it would require redesign of shear wall elements and the recalculation of Δ_s and Δ_m until the displacement performance was met.

Table 5.2 shows the ductility calculations for the three sets of panels. Ductility is determined by deviding the Δ_{SLS} by the Δ_{YLS}. This caluation can be deceiving because if F_{YLS} is equal to F_{SLS} (a flat-back bone curve), the ductility could be the same as an

element that has a greater F_{SLS} force than F_{YLS} force. A better way to measure the inelastic performance gains would be to determine the energy dissipation between the two elements. The energy dissipation of the element where F_{SLS} is greater would be the larger of the two.

Energy dissipation for each group of panels was calculated and the results are shown in Table 5.2 and Figure 5.15. The energy dissipation was determined by calculating the area under the combined force deformation curves as shown in Figure 5.14 ($A_1 + A_2 + A_3$). Figure 5.14 shows the combined bilinear force deformation curves for the two sets of 4′ panels sets 1 and 2 from Table 5.2. The YLS and SLS points, and the areas calculated for the energy dissipation of set 2 (Set 1 was not shown for clarity) are shown in Figure 5.15. The results of the calcualtions are in Table 5.2 and the increase from set 1 to set 2 is substantial. From Set 1 to Set 2 the energy dissipation increase is almost 100%. This increase is the most important factor demonstrated from all of the test results. The panels with the modifications demonstrated on panels 7 and 9 will have a 95% increase in energy dissipation. This would not be recogized under current code calculations; only a higher design force would be determined. The design force is a function of both Δ_{SLS} and F_{SLS}. Since seismic induced stresses are reversible, nonlinear, and time dependent, a symetric energy dissipation shear wall with symetric energy dissipation properties will enhance the structure's performance and compensate for building code design shortfalls.

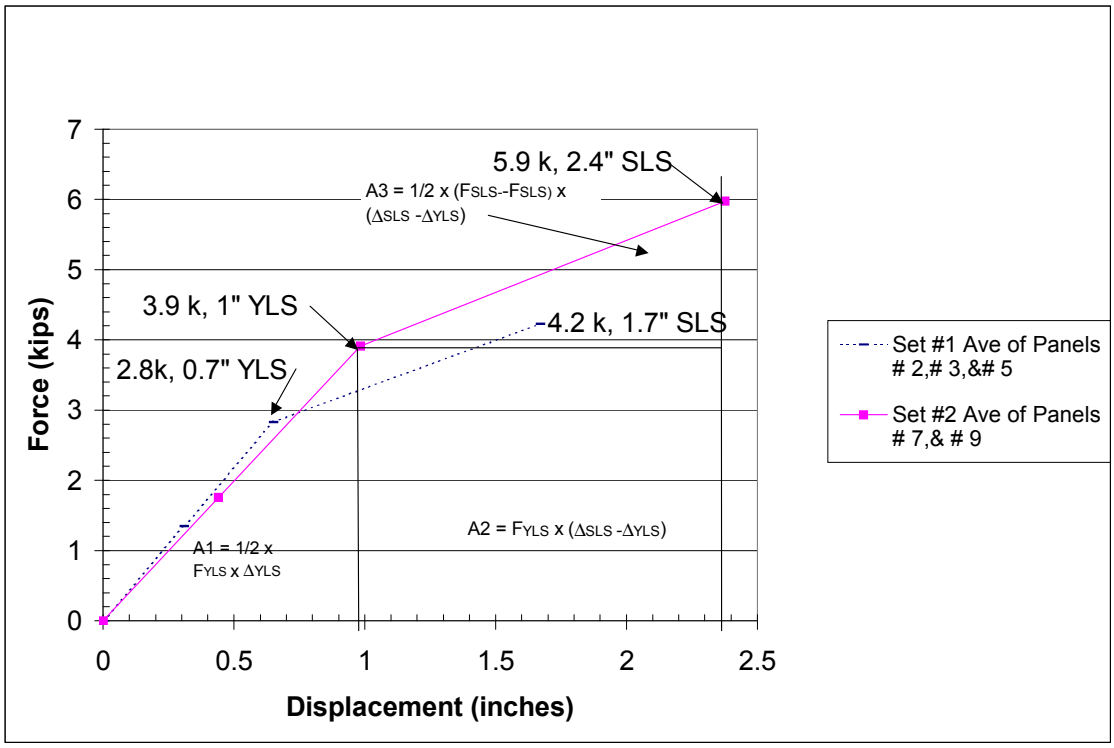

Figure 5.15. AC130 force deformation bilinear segments.